DYNAMIC MODAL ANALYSIS AND OPTIMIZATION OF THE WHEEL-SIDE REDUCER COVER BASED ON ANSYS

Yan ZHANG[1]

Electric forklifts are essential loading tools in the warehousing and logistics industry. The cover of the brake unit reducer on these forklifts is subject to intense vibration during operation, leading to resonance, noise, and fatigue damage issues. To address these problems, a dynamic modal analysis is conducted. A finite element model of the cover is created using ANSYS software, and modal analysis is performed to determine the cover's natural frequencies and corresponding vibration modes. Modal analyses are conducted specifically for the vibration-prone conditions of forklift startup and braking. The modal simulation results for these two conditions are compared with experimental data to verify the accuracy of the simulation. The results show that the simulation data are largely consistent with the experimental data, with resonance occurring under braking conditions. Improvement measures to avoid resonance are proposed, leading to successful optimization. This optimization prevents resonance in the cover, enhancing the operational stability of the wheel-side reducer and providing theoretical support for the design of the cover.

Keywords: ANSYS; Wheel-side reduce; Cover; Modal analysis; Optimization

1 Introduction

As a widely used transport vehicle in logistics warehouses in China, three-point electric forklifts have significant advantages. They are not only low in fuel consumption but also feature ease of maintenance and high operational efficiency. These characteristics play a crucial role in enhancing the production efficiency of logistics warehouses and the overall economic benefits of enterprises [1].

With the extensive application of three-point electric forklifts, the study of the wheel-side reducer's planetary gear system has been extensive and has matured. However, there is less research on the stress state of the wheel-side reducer cover, and there is still a lack of effective means to improve the damage under its working conditions. Therefore, improving the working state of the wheel-side reducer cover has become a research focus [2]. In recent years, scholars at home and abroad have studied the cover of the wheel-side reducer of electric forklifts. Zou Xihong et al [3] took the differential cover of an electric vehicle drive assembly as the research object, established a finite element model, conducted modal simulation analysis, and carried out experimental verification, conducting a dynamic simulation analysis

[1] Associate Professor, Anhui Vocational College Of Defense Technology, Anhui, China. e-mail: 285944530@qq.com.

of the differential housing; Li Shuaiqi et al [4] carried out static and modal analysis of the differential cover under extreme conditions and optimized the mass and dynamic and static characteristics of the differential cover; Syam Thaer et al [5] . conducted modal analysis through ANSYS and numerical analysis of the problem through finite element simulation, in addition, calculating stiffness based on the natural frequency and mass of the gear.

As a key component of the reducer, the cover is directly connected to the electric forklift's frame. During the operation of the electric forklift, the cover is affected by external conditions such as road undulations and changes in driving speed under different working conditions, as well as by excitations from internal sources such as the drive motor and transmission gear system [6]. When these excitations from multiple sources are superimposed, their vibration frequencies may coincide or approach the natural frequency of the cover, causing resonance in the cover. This phenomenon not only generates significant noise but also affects the driving stability and service life of the electric forklift [7].

Addressing the issues faced by the cover during operation, this paper conducts modal analysis of the cover using ANSYS software, compares the simulation results with experimental results to verify the accuracy of the simulations, and carries out optimizations based on the results, thus avoiding or reducing the likelihood of resonance in the cover. Therefore, conducting modal analysis of the electric forklift wheel-side reducer cover and making improvements and optimizations are of great significance for enhancing the reliability of the product.

2 Modal Analysis Theory

2.1 Modal Analysis Theory

With the advancement of technology, the performance requirements for electric forklifts have increased, leading to higher working speeds. Simple statics and empirical design are no longer sufficient to meet design requirements, necessitating vibration and dynamic performance analysis of key components of the reducer. Modal analysis, which has gradually developed since the 1960s, addresses many issues in dynamics characteristics and modal parameter identification that are difficult to analyze through statics. Modal analysis applies system identification to engineering vibrations, enabling the determination of a system's natural frequencies and mode shapes either through computer analysis or experimental methods. It also predicts vibration characteristics under resonance conditions, avoiding the operational frequency of the machinery and preventing resonance, which is of great importance for the stability of electric forklift operations. Regardless of the damping conditions, for a linear system with n degrees of freedom, its motion differential equation is:

$$[M]\{\ddot{x}(t)\} + [C]\{\ddot{x}(t)\} + [K]\{x(t)\} = \{F(t)\} \quad (1)$$

Where $[M]$ is the mass matrix; [C] is the damping matrix; $[K]$ is the stiffness matrix; $\ddot{x}(t)$ is the acceleration vector; $\{x(t)\}$is the displacement vector; $F(t)$ is the external excitation force vector.

When $\{F(t)\} = 0$, the equation simplifies to a homogeneous equation system with zero damping:

$$[M]\{\ddot{x}(t)\} + K\{x(t)\} = 0 \quad (2)$$

The solution to $\{F(t)\}$ is in the form of:

$$\{x(t)\} = \{x\}e^{jwt} = 0 \quad (3)$$

Substituting the expression into the equation, we get:

$$([K] - w^2[M])\{X\}e^{jwt} or([K] - w^2[M])\{X\} = 0 \quad (4)$$

Equation (4) is a homogeneous linear equation system. For this equation to have a non-zero solution, the coefficient determinant must be zero, i.e.:

$$([K] - w^2[M]) = 0 \quad (5)$$

It is an algebraic equation of order n in w^2. For a linear system with n degrees of freedom, there exist n distinct positive roots w_i *(i =1,2,..., n)*, which are arranged in ascending order: *0*< w_1 < w_2 <... w_n. Here, w_i is the modal frequency of the i-th mode, also known as the modal frequency.

2.2 Modal Analysis Calculation Methods

There are various modal calculation methods such as the block Lanczos method, PCG Lanczos method, unsymmetric method, damped method, supernode method, and others. In ANSYS, a sparse matrix solver is automatically used, employing the block Lanczos method for modal calculations.

The block Lanczos method has a relatively simple calculation formula and program, with high computational accuracy and requiring fewer storage units during the computation process. However, when dealing with complex structural models, the computational speed decreases and requires more storage units. Hence, the block Lanczos method is suitable for processing models with simple structures. For models with ill-conditioned matrices, the block Lanczos method can also yield satisfactory results, but it demands higher computer hardware capabilities, utilizing substantial memory during operation and slowing down computation speed. It is generally used for multi-order modal solutions with a large number of degrees of freedom.

The block Lanczos solver in the sparse matrix solver offers two different methods to solve for eigenvalues. The system chooses the faster method based on the set parameters. If no boundary conditions are set in the analysis, there will be an eigenvalue of size zero on each rigid body motion degree of freedom of the model [8].

3 Establishment of Finite Element Model

Based on the actual dimensions of the reducer, I used the 3D modeling software Pro/E to create a three-dimensional model of the reducer and its cover. To facilitate modal simulation calculations, the 3D model of the cover was simplified. The model's surface has many bolt holes. During the assembly phase, interference checks between the bolt holes were conducted to ensure that the model would not affect the finite element analysis when imported into the analysis software. Finally, the established three-dimensional model of the cover was imported into ANSYS as an *"x_t"* format file [9]. The main steps in conducting modal analysis of mechanical structures are as follows:

(1) When setting material properties, this paper requires defining parameters such as the part's density, Poisson's ratio, and elastic modulus [10]. For the wheel-side reducer cover, its material properties are as follows: The part is made of HT400 material, which can withstand a maximum stress value of 81.2 MPa and has a strain limit of 0.028 mm. Its Poisson's ratio is 0.26, density is 8.0 g/cm³, and it is subjected to gravitational acceleration of 9.8 m/s. Finally, its modulus of elasticity is 160 GPa.

(2) The contact area refers to the region where two objects are in contact during relative motion. In this definition, the contact area between the cover and the output shaft is defined as non-separable contact because they are in a relative rotational motion. This means that they will not separate in the contact area, even though they can move relative to each other elsewhere [11]. On the other hand, the connection between the cover and the connecting bolts is a fixed connection, so their interaction is defined as bonded. This means that the motion of the cover and connecting bolts in the model is bound together, and they will not move relative to each other [12].

(3) Before mesh division, this paper first simplified the reducer cover model. Following the principle of simplification, features with little impact on the overall structure were removed, such as non-load-bearing parts, holes with diameters less than 6 mm, lubrication holes not involved in the connection, and chamfers with distances less than 1.5 mm [13]. After simplification, the model structure became relatively simple, without overly complex manufacturing processes. Despite the cover's surface presenting an irregular curved shape, this paper still used automatic mesh division to divide the mesh. After the division, the entire model generated a total of 124,106 nodes and 77,580 elements. These nodes and cells will provide basic data for subsequent finite element analysis [14].

(4) During the operation of ANSYS, to simulate the actual working state of the cover, it is necessary to apply boundary conditions and loads to it. Based on the working principle of the cover, this paper chose to apply full constraints at both ends of the cover to ensure that it does not undergo any displacement or motion during loading. This method of constraint can accurately simulate the constraint

conditions of the cover during actual work, thereby obtaining more accurate analysis results [15].

Based on the above steps, the created model is shown in Figs 1, 2, and 3:

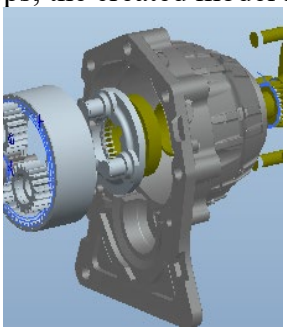

Fig. 1. 3D assembly diagram of the reducer

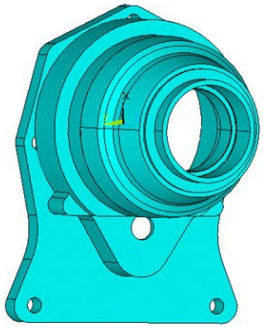

Fig. 2. Simplified model of the cover

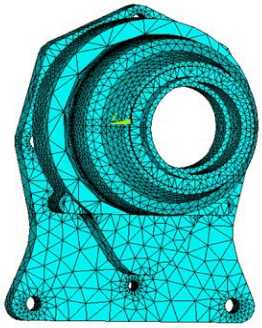

Fig. 3. Finite element model of the cover

4 Modal Analysis of the Reducer Cover

Modal analysis is an important method for studying the vibration characteristics of mechanical structures. Its main research objects include key parameters such as natural frequencies and mode shapes, which are important bases for mechanical structures to bear dynamic loads. Through modal analysis, this study can determine the natural frequencies of components, thereby avoiding these

frequencies during the design process or minimizing the excitation at these frequencies to eliminate excessive vibration and noise. Therefore, modal analysis is of great significance for improving the stability and reliability of mechanical structures [16].

4.1 Natural Frequencies and Mode Shapes

In the process of modal analysis, high-order modes have relatively less impact on the dynamic characteristics of the cover's mechanical structure, while low-order modes play a more critical role. Therefore, in solving for modes, this study set the solution results to the first 20 modes. This setting can more accurately reflect the dynamic characteristics of the mechanical structure and is helpful for optimization design [17].

By importing the finite element model of the cover into the modal analysis module of ANSYS software for analysis, the first 20 constrained modes of the cover were calculated, obtaining the natural frequencies and mode shapes for the first 20 orders, as shown in Fig. 4.

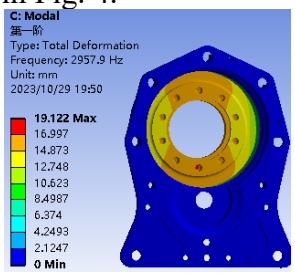

(a) First order natural mode shape

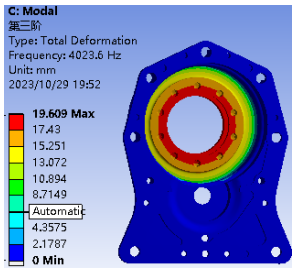

(b) Third order natural mode shape

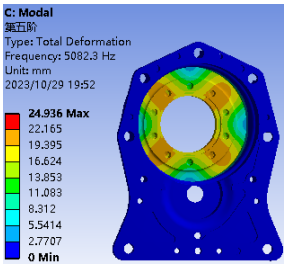

(c) Fifth order natural mode shape

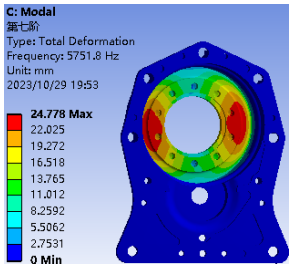

(d)Seventh order natural mode shape

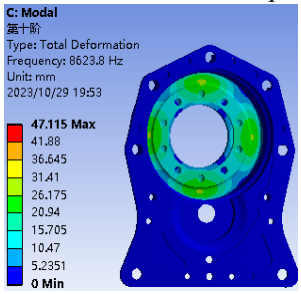

(e) Tenth order natural mode shape

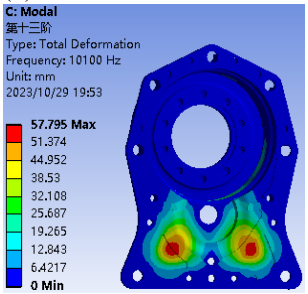

(f) Thirteenth order natural mode shape

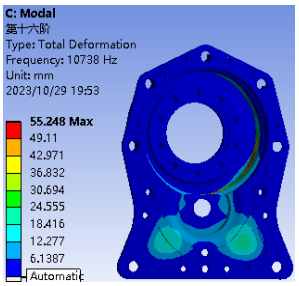

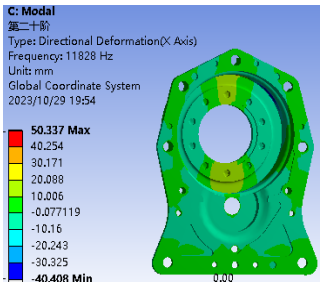

(g) Sixteenth order natural mode shape (h) Twentieth order natural mode shape

Fig. 4. Mode shapes of various orders of the cover

Table 1

Natural frequencies of various orders of the cover

Modal Order	Natural Frequency (Hz)	Modal Order	Natural Frequency (Hz)
1	2957	11	9468
2	2960	12	9772
3	4023	13	10100
4	4095	14	10184
5	5082	15	10496
6	5741	16	10738
7	5751	17	10800
8	6235	18	11267
9	8574	19	11521
10	8623	20	11828

From the mode shapes and Table 1, it can be seen that the natural frequencies of the cover are quite high, with the lowest order natural frequency being 2957 Hz. From the first to the twentieth order, the natural frequencies show an increasing trend [18].

4.2 Modal Analysis under Operating Conditions

The cover is mainly subject to internal and external excitations. The internal excitation mainly comes from the planetary gear set, and due to the smooth transmission of the reducer gear set, the excitation can be considered negligible. External excitation arises from road surface vibration and the rotational speed of the AC drive motor. As the working environment of the electric forklift is the flat floor of a logistics warehouse, the road surface excitation can also be ignored. Therefore, in the analysis process, only the external excitation caused by the

rotational speed of the AC drive motor under different conditions needs to be considered [19].

The operation of the electric forklift is mainly divided into three conditions: starting, cruising, and braking. The power of the AC drive motor is 6 kW with a rated speed of 1500 r/min, and the motor speed in the cruising condition is 1000 r/min. The frequencies of various orders are only up to 643 Hz, which is far below the minimum value of the cover's natural frequencies. Thus, when the electric vehicle operates in cruising conditions, the external excitation to the cover is minimal and does not cause resonance [20].

Under starting and braking conditions, due to the sudden speed change of the electric forklift, the AC drive motor may experience unstable speeds. Through the ANSYS modal analysis module, an analysis of the cover under actual working conditions is conducted. The focus is on analyzing the spatial displacement curves of the most displacement-prone and resonance-prone 13th node on the cover in the first to the twentieth mode under both starting and braking conditions, as shown in Fig. 5. and Fig. 6. These figures depict the amplitude and frequency of the 13th node in the X, Y, and Z directions of the coordinate system under the two conditions [21].

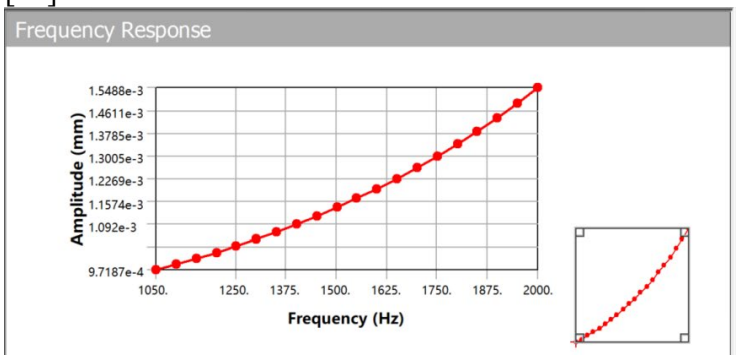

	Frequency [Hz]	Amplitude [mm]
1	1050.	9.7187e-004
2	1100.	9.8535e-004
3	1150.	9.9988e-004
4	1200.	1.0155e-003
5	1250.	1.0324e-003
6	1300.	1.0506e-003
7	1350.	1.0701e-003
8	1400.	1.0913e-003
9	1450.	1.1141e-003
10	1500.	1.1388e-003
11	1550.	1.1655e-003
12	1600.	1.1945e-003
13	1650.	1.226e-003
14	1700.	1.2603e-003
15	1750.	1.2977e-003
16	1800.	1.3387e-003

(a) X-direction displacement graph

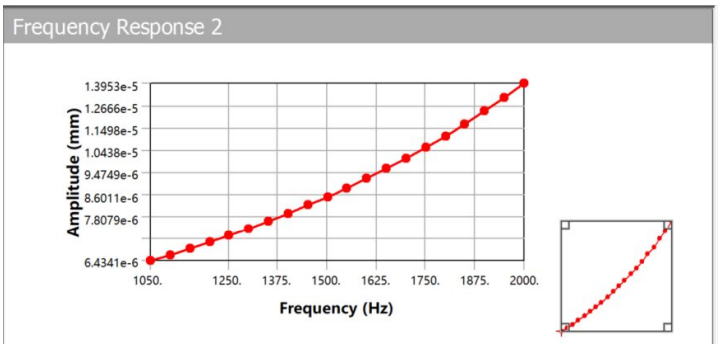

	Frequency [Hz]	Amplitude [mm]
1	1050.	6.4341e-006
2	1100.	6.6001e-006
3	1150.	6.7795e-006
4	1200.	6.9732e-006
5	1250.	7.1826e-006
6	1300.	7.4089e-006
7	1350.	7.6538e-006
8	1400.	7.9189e-006
9	1450.	8.2061e-006
10	1500.	8.5179e-006
11	1550.	8.8567e-006
12	1600.	9.2256e-006
13	1650.	9.628e-006
14	1700.	1.0068e-005
15	1750.	1.055e-005
16	1800.	1.108e-005

(b) Y-direction displacement graph

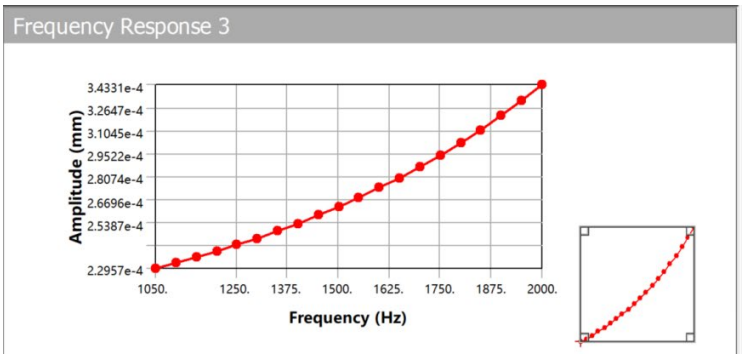

	Frequency [Hz]	Amplitude [mm]
1	1050.	2.2957e-004
2	1100.	2.3227e-004
3	1150.	2.3517e-004
4	1200.	2.383e-004
5	1250.	2.4166e-004
6	1300.	2.4528e-004
7	1350.	2.4918e-004
8	1400.	2.5338e-004
9	1450.	2.5791e-004
10	1500.	2.628e-004
11	1550.	2.6809e-004
12	1600.	2.7382e-004
13	1650.	2.8003e-004
14	1700.	2.8679e-004
15	1750.	2.9415e-004
16	1800.	3.022e-004

(c) Z-direction displacement graph

Fig. 5. X, Y, Z direction displacement graphs of node 13 under starting condition

From Fig. 5, it can be seen that the frequencies of the 1st to 20th orders for the displacement-prone node 13 range from 1050 Hz to 2000 Hz, and the frequencies gradually increase with the order, as do the displacements in the X, Y, and Z directions. The lowest value of the natural frequency is 2957 Hz. It is only when the node 13 reaches a certain order that the frequency may reach the lowest area of the natural frequency, so the probability of resonance is low.

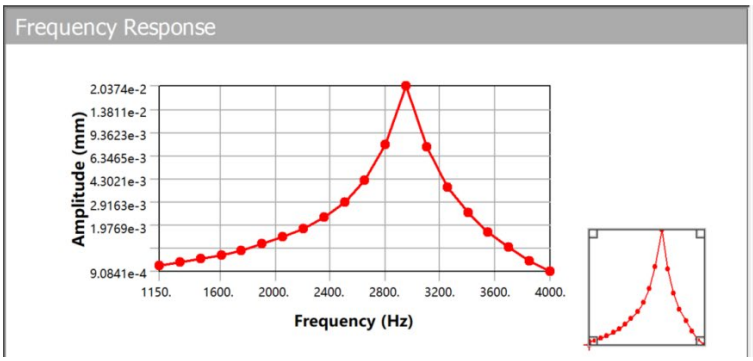

	Frequency [Hz]	Amplitude [mm]
1	1150.	9.9972e-004
2	1300.	1.0503e-003
3	1450.	1.1137e-003
4	1600.	1.1939e-003
5	1750.	1.2968e-003
6	1900.	1.4318e-003
7	2050.	1.6144e-003
8	2200.	1.8724e-003
9	2350.	2.261e-003
10	2500.	2.9068e-003
11	2650.	4.1742e-003
12	2800.	7.6448e-003
13	2950.	2.0374e-002
14	3100.	7.2864e-003
15	3250.	3.7072e-003
16	3400.	2.4136e-003

(a) X-direction displacement graph

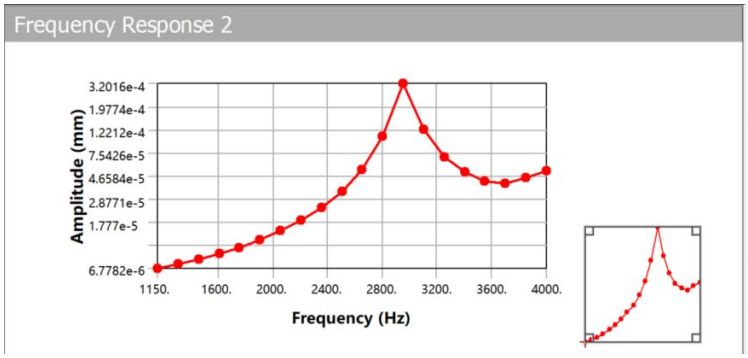

	Frequency [Hz]	Amplitude [mm]
1	1150.	6.7782e-006
2	1300.	7.407e-006
3	1450.	8.2031e-006
4	1600.	9.2208e-006
5	1750.	1.0542e-005
6	1900.	1.2339e-005
7	2050.	1.4877e-005
8	2200.	1.8533e-005
9	2350.	2.4146e-005
10	2500.	3.367e-005
11	2650.	5.2802e-005
12	2800.	1.069e-004
13	2950.	3.2016e-004
14	3100.	1.2352e-004
15	3250.	6.8662e-005
16	3400.	5.0117e-005

(b) Y-direction displacement graph

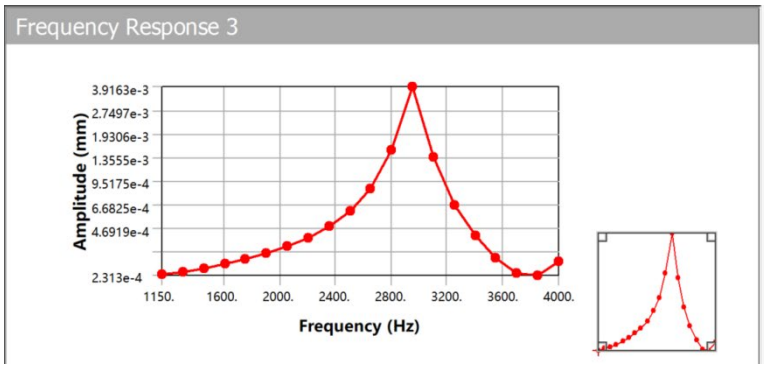

	Frequency [Hz]	Amplitude [mm]
1	1150.	2.3514e-004
2	1300.	2.4523e-004
3	1450.	2.5783e-004
4	1600.	2.737e-004
5	1750.	2.9397e-004
6	1900.	3.2044e-004
7	2050.	3.5607e-004
8	2200.	4.0621e-004
9	2350.	4.8142e-004
10	2500.	6.0593e-004
11	2650.	8.495e-004
12	2800.	1.5144e-003
13	2950.	3.9163e-003
14	3100.	1.3552e-003
15	3250.	6.6618e-004
16	3400.	4.2011e-004

(c) Z-direction displacement graph

Fig. 6. X, Y, Z direction displacement graphs of node 13 under braking condition

From Fig. 6, it is apparent that in the braking condition, the frequencies of the 1st to 20th orders for node 13 range from 1150 Hz to 4000 Hz, with the frequency range gradually increasing with order. There is an overlap in the frequency range with the natural frequency, indicating a high probability of resonance. The displacement graphs in the X, Y, and Z directions show a sudden increase in displacement values from the 11th to the 14th order, indicating the occurrence of resonance. When the working vibration frequency reaches its natural frequency, the vibration amplitude far exceeds its allowable displacement amount, which could lead to the structural damage of the cover and directly affect the normal functioning of the wheel-side reducer.

4.3 Experimental Validation

Before optimization, the accuracy of the modal analysis simulation data was verified through experimental methods. The data input for experimental validation was derived from the modal analysis results. The vibration amplitude of the 13th node, located in the output shaft bearing area with the most displacement, was identified as a major area of concern, and most test points were distributed in this area, reducing the number of test points in other less critical areas.

The stress hammer method was used for testing the starting and braking conditions. Ten main test points on the output shaft bearing were excited, and data was collected through sensors on 15 test points on the cover. The vibration signal curves and corresponding data for the first to twentieth orders under both conditions were obtained, as shown in Fig. 7.

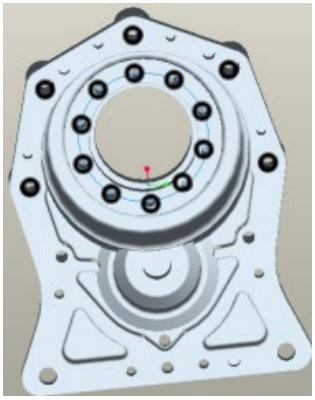

(a) Test point diagram

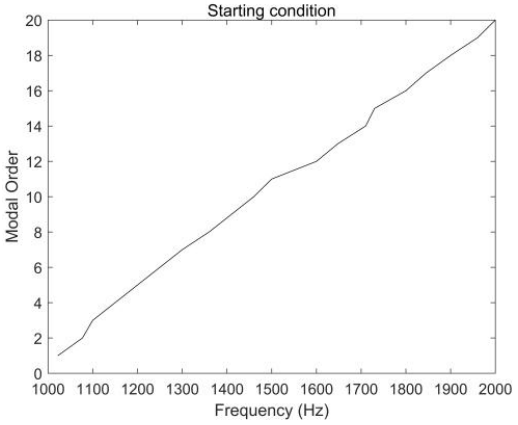

(b) Frequency curve under starting condition

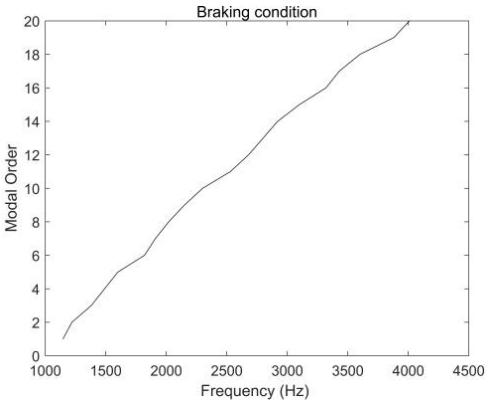

(c) Frequency curve under braking condition

Fig. 7. Test diagrams

Based on the collected data, a comparison of experimental and simulation results is shown in Table 2.

Table 2

Comparison of Test and Simulation Results (Only the first ten orders are shown due to space constraints)

Modal Order	Test Result (Hz) Starting Condition	Simulation Result(Hz) Starting Condition	Test Result(Hz) Braking Condition	Simulation Result(Hz) Braking Condition
1	1146	1150	1022	1050
2	1220	1300	1077	1100
3	1380	1450	1100	1150
4	1490	1600	1150	1200
5	1600	1750	1200	1250
6	1820	1900	1250	1300
7	1910	2050	1300	1350
8	2020	2200	1360	1400
9	2150	2350	1410	1450
10	2300	2500	1460	1500

The comparison of test values and simulation results in Table 2 shows that the error range is within 8%. The simulation results are broadly consistent with the test results, confirming the accuracy and validity of the modal simulation analysis, which lays the groundwork for subsequent optimization.

5 Optimization and Improvement

Modal analysis of the three conditions indicated that the highest probability of resonance occurred in the braking condition. A series of optimizations were then applied, followed by another modal analysis in ANSYS under the braking condition. According to the literature, there are generally two ways to optimize: changing the shape and arrangement of the cover parts or improving the stiffness of the cover material. The first option is not feasible as changing the cover's shape or component arrangement would require modifications to the output shaft, cover plate, and end cover, leading to extensive changes[21]. The second option, improving material stiffness, can be achieved by either using higher quality materials or increasing the thickness of the cover in certain areas. Since the cover accounts for half of the reducer's volume and weight, replacing it with higher quality material would be cost-prohibitive. Thus, the best choice is to increase the thickness locally. The area most prone to resonance is the inner ring of the bearing at node 13, which originally had a thickness of 6 mm. Increasing the thickness by 3 mm, while ensuring economy and lightweight, was deemed appropriate. After optimization, the improved model was recalculated under the braking condition following the modal analysis steps, yielding the following results:

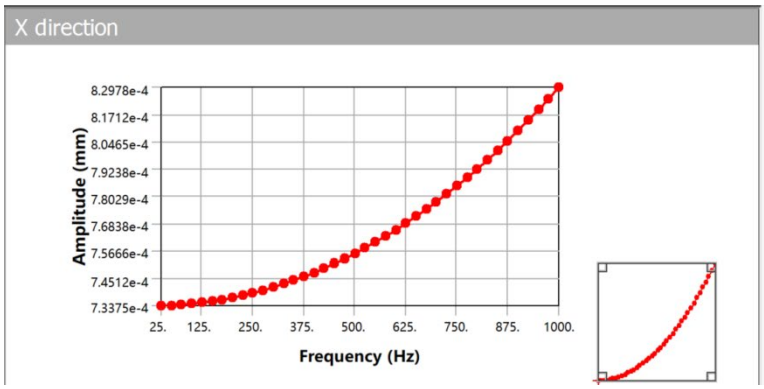

	Frequency [Hz]	Amplitude [mm]
1	25.	7.3375e-004
2	50.	7.3391e-004
3	75.	7.3417e-004
4	100.	7.3455e-004
5	125.	7.3503e-004
6	150.	7.3561e-004
7	175.	7.3631e-004
8	200.	7.3711e-004
9	225.	7.3803e-004
10	250.	7.3905e-004
11	275.	7.4018e-004
12	300.	7.4143e-004
13	325.	7.4279e-004
14	350.	7.4426e-004
15	375.	7.4585e-004
16	400.	7.4756e-004

(a) X-direction displacement graph

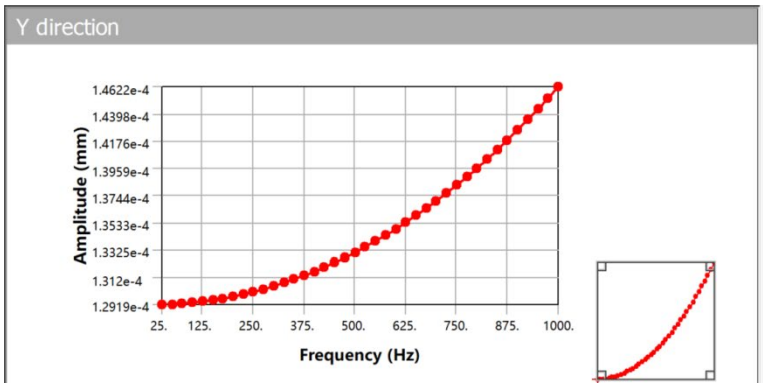

	Frequency [Hz]	Amplitude [mm]
1	25.	1.2919e-004
2	50.	1.2922e-004
3	75.	1.2926e-004
4	100.	1.2933e-004
5	125.	1.2942e-004
6	150.	1.2952e-004
7	175.	1.2964e-004
8	200.	1.2979e-004
9	225.	1.2995e-004
10	250.	1.3013e-004
11	275.	1.3033e-004
12	300.	1.3055e-004
13	325.	1.3079e-004
14	350.	1.3106e-004
15	375.	1.3134e-004
16	400.	1.3164e-004

(b) Y-direction displacement graph

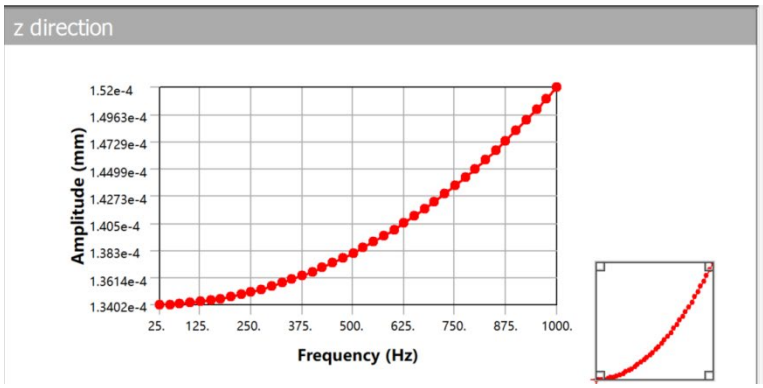

	Frequency [Hz]	Amplitude [mm]
1	25.	1.3402e-004
2	50.	1.3405e-004
3	75.	1.341e-004
4	100.	1.3417e-004
5	125.	1.3426e-004
6	150.	1.3437e-004
7	175.	1.345e-004
8	200.	1.3465e-004
9	225.	1.3482e-004
10	250.	1.3501e-004
11	275.	1.3522e-004
12	300.	1.3545e-004
13	325.	1.3571e-004
14	350.	1.3598e-004
15	375.	1.3628e-004
16	400.	1.366e-004

(c) Z-direction displacement graph

Fig. 8. X, Y, Z direction displacement graphs of node 13 under braking condition after optimization

As shown in Fig. 8, after optimization, the frequencies of the 1st to 20th orders of node 13 under the braking condition were a maximum of 500 Hz, significantly lower than the lowest natural frequency of 2957 Hz. The

displacements in the X, Y, and Z directions were minimal and within normal ranges, effectively preventing resonance.

6 Conclusion

Based on the intrinsic frequencies of the cover, modal analysis revealed that during braking conditions, the actual operating frequencies of the cover overlapped with its natural frequencies. This overlap led to transient increases in displacement values and resonance, causing increased noise and reduced operational stability in electric forklifts during braking, and damaging the cover. Experimental validation confirmed the accuracy and effectiveness of the modal analysis. Drawing on scholars' experiences, optimizations were made to the cover. The optimized cover's frequency and displacement were within the specified range, eliminating the occurrence of resonance. Through modal analysis and subsequent optimization based on the analysis results, the reliability of the wheel-side reducer's operation was significantly improved, thereby extending the lifespan of electric forklifts. This has substantial implications for the economic development of the logistics industry.

The study of the cover's operational state mainly includes dynamic modal analysis and static analysis. This paper carried out the dynamic modal analysis of the cover, and further static studies will be continued in the future. Considering cost-effectiveness, this paper only optimized the thickness of the inner ring of the output shaft bearing. Future optimizations could include changing materials or modifying the shape and arrangement of the cover and its components. Subsequent analyses will provide more comprehensive data, offering greater guidance for the design, manufacturing, and use of wheel-side reducers.

Acknowledgement

This work was supported by the 2023 Anhui Province Vocational Education Project (AZCJ2023024) and the 2023 Key Research Projects of the College (gf2023jxyjz02).

REFERENCES

[1]. *Wang Wenbin, Wang Hui, Duan Cunhu, Liu Hua,* "Modal Analysis and Test Verification of Mining Dump Truck Frame", in Coal Mine Machinery, **vol. 44**, no. 11, Oct. 2023, pp. 44-46

[2]. *Yang Qin, Liu Daoxiu, Zhao Xiaotao,* "Modal Analysis of Cone Crusher Moving Cone Based on ANSYS", in MECHANICAL & ELECTRICAL ENGINEERING TECHNOLOGY, **vol. 52**, no. 9, Sep. 2023, pp. 105-109

[3]. *Zou XiHong, Gou LinLin, Xiong Feng, WANG Chao, Jiang MingCong,* "Fatigue life analysis of differential case of elect drive assembly based on actual load spectrum", in Journal of Mechanical Strength, **vol. 45**, no. 1, Feb. 2023, pp. 228-236

[4]. *Li Shuaiqi, Guan Dianzhu, Chen Yang,* "Finite Element Analysis and Multi-objective Optimization of Differential Housing", in MECHANICAL ENGINEERING & AUTOMATION, **vol. 200**, no. 1, Feb. 2017, pp. 52-54

[5]. *Syam Thaer, Badri Yousif, Renno Jamil,* "Modal analysis of spur gears for varied teeth root cracks characteristics: finite element analysis (FEA) simulations", in Vibroengineering PROCEDIA, **vol. 383**, no. 1, Jan. 2022, pp. 33-40

[6]. *Helal Mahmoud, Fathallah Elsayed,* "Finite element analysis and design optimization of a non-circular sandwich composite deep submarine pressure hull", in Materials Testing, **vol. 62**, no. 10, Nov. 2020, pp. 1025-1032

[7]. *Stanisław Burzyński,* "On FEM analysis of Cosserat-type stiffened shells: static and stability linear analysis", in Continuum Mechanics and Thermodynamics, 2020, pp. 1-26

[8]. *Chen Qisheng, Zhang Hongmei, Zhao Xuzhi,* "Research on Statics and modal analysis of press combined fuselage", in China Metalforming Equipment & Manufacturing Technology, **vol. 56**, no. 6, Dec. 2021, pp. 7-12

[9]. *Kim JinJae, Bae Moonki, Hong MyoungPyo, Kim YoungSuk,* "Finite Element Analysis on Welding-Induced Distortion of Automotive Rear Chassis Component", in Metals, **vol. 12**, no. 2, Feb. 2022, pp. 287-293

[10]. *Ali Aidy, Faidzi M.K., Kamarudin Khairul H., Abdullah M.F., Saad M.R.,* "Simulation and Experimental of Crack Propagation in Automotive Engineering Component", in Key Engineering Materials, **vol. 6289**, Feb. 2022, pp. 467-472

[11]. *Hamzi Nazirul Muhaimin, Singh Salvinder, Abdullah Shahrum, Rasani Mohammad Rasidi,* "Fatigue life assessment of vehicle coil spring using finite element analysis under random strain loads in time domain", in International Journal of Structural Integrity, **vol. 13**, no. 4, Jul. 2022, pp. 685-698

[12]. *Sivaprakasam Palani, Abebe Esayas, Čep Robert, Elangovan Muniyandy ,* "Thermo-Mechanical Behavior of Aluminum Matrix Nano-Composite Automobile Disc Brake Rotor Using Finite Element Method", in Materials, **vol. 15**, no. 17, Sept. 2022, pp. 6072-6072

[13]. *V R Deulgaonkar, S Deshpande, A Bengle, P Dhanawade,* "Finite Element Analysis of Foldable Electric Vehicle", in International Journal of Vehicle Structures & Systems, **vol. 14**, no. 6, Jan. 2022, pp. 697-702

[14]. *Egner Felix Simeon, Wang Yonggang, Willems Thijs, Kirchner Matteo,* "High-Speed Camera based Experimental Modal Analysis for Dynamic Testing of an Automotive Coil Spring", in SAE International Journal of Advances and Current Practices in Mobility, **vol. 4**, no. 1, Aug. 2021, pp. 278-288

[15]. *A. Balakrishna, P.K. Mishra,* "Modelling and analysis of static and modal responses of leaf spring used in automobiles", in International Journal of Hydromechatronics, **vol. 4**, no. 4, Jan. 2021, pp. 350-367

[16]. *AZAM PASHA A, Praveen D.N, Lohitesh Jaga Kumar,T.P. Bharathesh,*"Design and modal analysis of automotive crankshaft for material optimization using ANSYS workbench", in International Journal of Recent Trends in Engineering and Research, **vol. 5**, no. 8, Mar. 2020, pp. 59-67

[17]. *Li Xiaohua, He Wendan, Zhao Rongjian, Feng Anhui, Liu Yudong, Lu Yue,* "Modal analysis of the stator system of a permanent magnet synchronous motor with integer slot multi-pole pair for electric vehicles", in IET Electric Power Applications, **vol. 16**, no. 1, Nov. 2021, pp. 1-14

[18]. *Garafolo Nicholas Gordon, Farhad Siamak, Koricherla Manindra Varma, Wen Shihao, Esmaeeli Roja,* "Modal Analysis of a Lithium-Ion Battery for Electric Vehicles", in Energies, **vol. 15**, no. 13,Jul. 2022, pp. 4841-4841

[19]. *Gaute Alonso Alvaro, Garcia Sanchez David, Ramos Gutierrez Óscar Ramón,* "Novel method for an optimised calculation of modal analysis of girder bridge decks", in Scientific Reports, **vol. 12**, no. 1, Jul.2022, pp. 12500-12502

[20]. *Roberto Michel,* "Extending the life of electric trucks", in Modern Materials Handling, **vol. 78**, no. 1, Jan . 2023, pp. 10,12-13

[21]. *Forouzesh Farinaz, Ahmadian Hamid, Navidbakhsh Mahdi,* "A 3D finite element model updating of spinal lumber segment applying experimental modal data and particle swarm optimization algorithm", in Distributed Systems Eng., **vol. 29**, no. 19-20, 2023, pp. 4673-4686